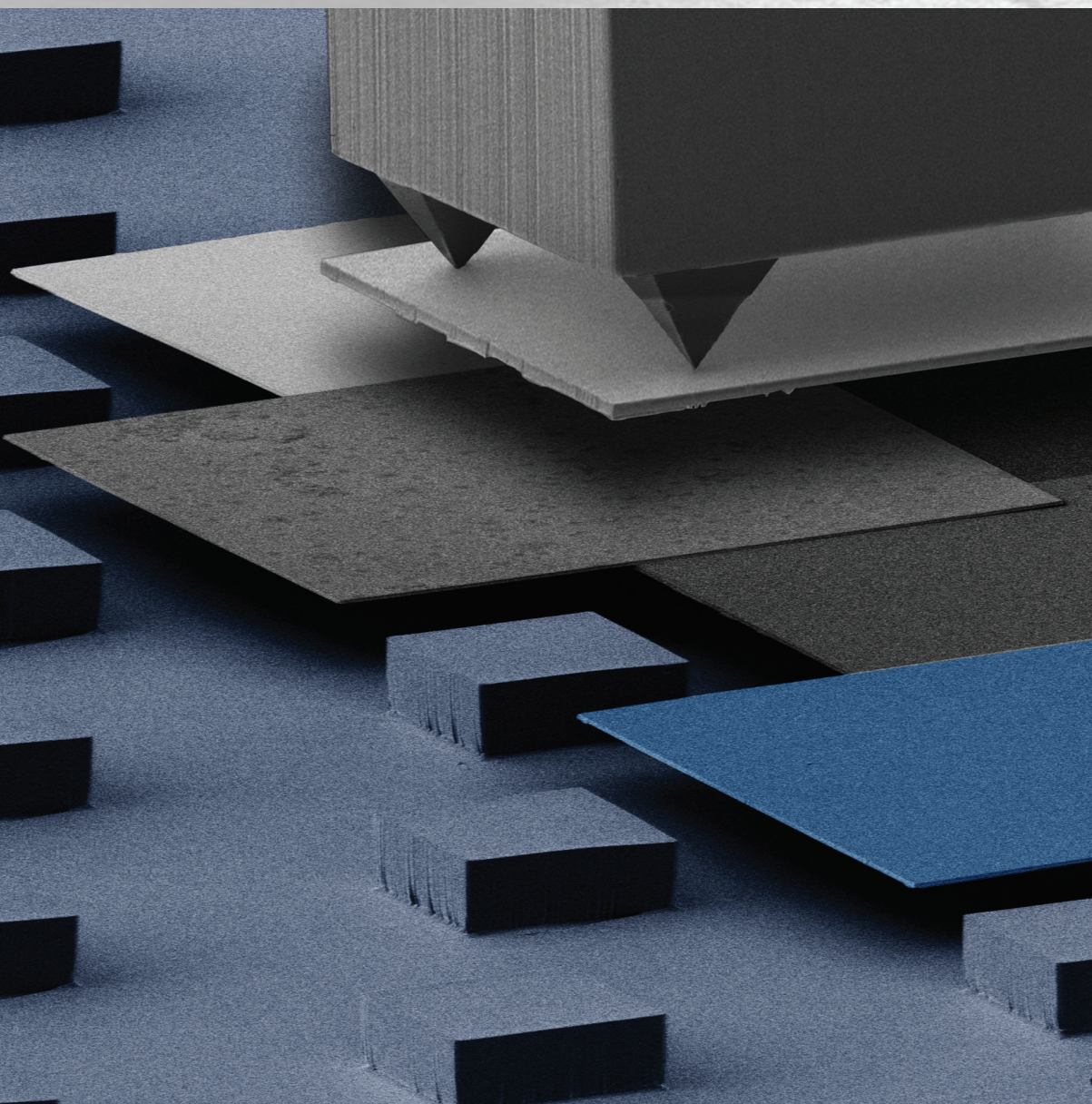


Volume 8 · No. 6 – March 26 2012

NANO **MICRO**

small

www.small-journal.com



6/2012

 **WILEY-VCH**

Imbricate Scales as a Design Construct for Microsystem Technologies

J. A. Rogers et al.

Imbricate Scales as a Design Construct for Microsystem Technologies

Seok Kim, Yewang Su, Agustin Mihi, Seungwoo Lee, Zhuangjian Liu, Tanmay K. Bhandakkar, Jian Wu, Joseph B. Geddes III, Harley T. Johnson, Yongwei Zhang, Jung-Ki Park, Paul V. Braun, Yonggang Huang, and John A. Rogers*

Spatially overlapping plates in tiled configurations represent designs that are observed widely in nature (e.g., fish and snake scales) and man-made systems (e.g., shingled roofs) alike. This imbricate architecture offers fault-tolerant, multifunctional capabilities, in layouts that can provide mechanical flexibility even with full, 100% areal coverages of rigid plates. Here, the realization of such designs in microsystems technologies is presented, using a manufacturing approach that exploits strategies for deterministic materials assembly based on advanced forms of transfer printing. The architectures include heterogeneous combinations of silicon, photonic, and plasmonic scales, in imbricate layouts, anchored at their centers or edges to underlying substrates, ranging from elastomer sheets to silicon wafers. Analytical and computational mechanics modeling reveal distributions of stress and strain induced by deformation, and provide some useful design rules and scaling laws.

1. Introduction

The surfaces of butterflies, fish, snakes, and other organisms have evolved to adapt to varied environments, by providing functions such as coloration^[1-2] for concealment or mimicry,

self-cleaning action^[3] with reduced adhesion/friction,^[4] and physical/chemical protection.^[5] A design construct often observed in such creatures involves discrete scales tethered to underlying, flexible skins. For example, wings of the

Prof. S. Kim, Dr. T. K. Bhandakkar, Prof. H. T. Johnson
Department of Mechanical Science and Engineering
University of Illinois at Urbana-Champaign
1206 West Green Street, Urbana, IL 61801, USA

Dr. Y. Su, Prof. Y. Huang
Department of Civil and Environmental Engineering
Department of Mechanical Engineering
Northwestern University
2145 Sheridan Road, Evanston, IL 61208, USA

Dr. A. Mihi, Dr. J. B. Geddes III, Prof. P. V. Braun
Department of Materials Science and Engineering
Beckman Institute for Advanced Science and Technology
University of Illinois at Urbana-Champaign
1304 West Green Street, Urbana, IL 61801, USA

Dr. S. Lee, Prof. J.-K. Park
Department of Chemical and Biomolecular Engineering
Korea Advanced Institute of Science and Technology
373-1, Guseong-dong, Yuseong-gu, Daejeon 305-701
Republic of Korea

Dr. Z. Liu, Dr. Y. Zhang
Institute of High Performance Computing
Fusionopolis Way, #16-16 Connexis, 138632, Singapore

Prof. J. Wu
Department of Engineering Mechanics
Tsinghua University
Beijing 100084, China

Prof. J. A. Rogers
Department of Materials Science and Engineering
Frederick Seitz Materials Research Laboratory
Beckman Institute for Advanced Science and Technology
University of Illinois at Urbana-Champaign
1304 West Green Street, Urbana, IL 61801, USA
E-mail: jrogers@uiuc.edu



DOI: 10.1002/sml.201101832

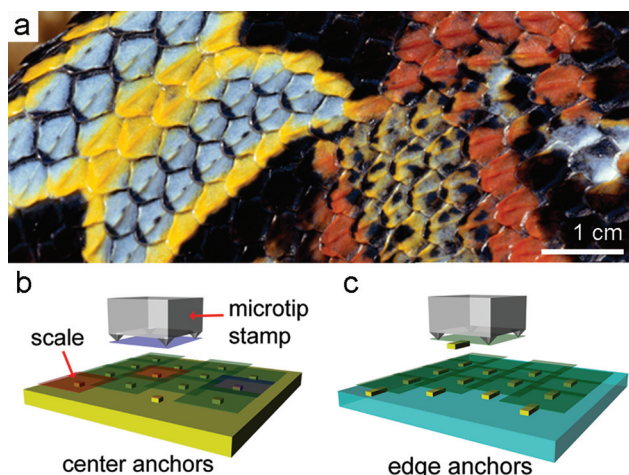


Figure 1. a) Optical microscopy image of scales of a snake (*Rhinoceros Adder*). Reproduced with permission.^[20] Copyright 2008, National Geographic. b,c) Schematic illustration of transfer printing procedures for forming assemblies of synthetic scales with anchors located in the centers (b) and edges (c).

Morpho butterfly^[1] support imbricate (i.e., spatially overlapping) scales, each of which displays diffractive coloration.^[2] See Figure S1 in the Supporting Information (SI). Similarly, scales of other butterflies offer reduced aerodynamic drag^[6] and facilitated cleaning in wet environments.^[3] A similar configuration in snakes enables full-area coverage of protective, hard scales with absorptive coloration, in a manner that affords the ability to stretch, flex, and deform to accommodate body motions. See **Figure 1a**. Man-made versions of this imbricate architecture appear in varied applications, ranging from roof shingles to armor plates in medieval knight cuirasses. Similar designs have not, however, been implemented in functional microsystems for electronics, optoelectronics, or photonics, in spite of several appealing features: 1) devices with such layouts can naturally incorporate highly fault-tolerant layouts, such that a failure at one scale has minimal effect on the operation of neighboring scales; 2) large-area systems can be constructed by combining scales derived from small 3D blocks of material; 3) multifunctional surfaces can be achieved by assembling heterogeneous collections of scales; and 4) the resulting systems can be integrated on rigid, flexible, or stretchable substrates, in planar or curvilinear geometries, even with full-area coverage of hard, rigid scales. Here, we describe the construction of imbricate architectures of silicon, photonic, and plasmonic scales on both soft (e.g., silicone slabs) and hard substrates (e.g., silicon wafers) using an advanced form of a transfer printing.^[7,8] The experimental results and associated finite-element models provide design rules for systems of this type, for which there are many potential areas of use.^[9–19]

2. Results

We explored several types of imbricate microsystems, each consisting of heterogeneous collections of silicon, photonic, and plasmonic scales. The fabrication process began

with creation of three different classes of scales on ‘source’ substrates, according to procedures described in detail in the Experimental Section. Undercut etching released the scales from these substrates along their bottom surfaces, in a scheme that included a thin layer of photoresist around their periphery, to hold them in their lithographically defined locations. Assembling these scales into imbricate architectures relied on a recent, advanced form of transfer printing, as described in detail elsewhere.^[8] Briefly, the process involved contact of a soft, elastomeric stamp of poly(dimethylsiloxane) (PDMS) with pyramidal features of relief (i.e., microtips) on its surface against the scales. Application of sufficient force collapsed the microtips, thereby yielding nearly full-area contact with the scales. Quickly peeling back the stamp fractured the photoresist structures, and removed the scales from the source substrate, leaving them attached by van der Waals interactions to the stamp surface.^[21] Shortly after, elastic restoring forces led to extension of the microtips back to their original geometries, leaving contact with the scales only at the sharp tips. This reversible mechanics of collapse and extension effectively switches the degree of adhesion of the scale to the stamp between strong and weak states, respectively. Gently contacting a target substrate, and then slowly retracting the stamp accomplished the transfer, to complete the process and to prepare the stamp for another cycle of printing. Repetitive application of these steps using automated printer tools enabled the integration of various types of scales in nearly any arrangement.

Two different possibilities were explored, schematically illustrated in Figure 1b,c. In the first, the target substrate consisted of a slab of PDMS molded with posts in a square array. Aligned transfer printing delivered scales to each post, in a sequential fashion. Bonding to the posts (i.e., anchors) was

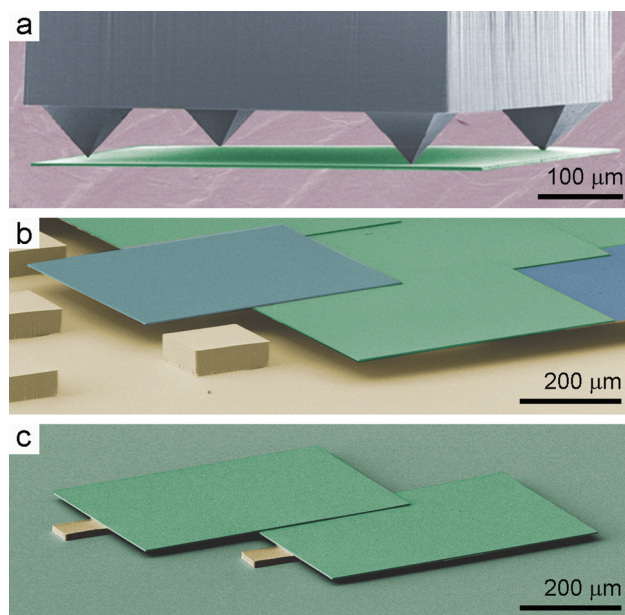


Figure 2. Colorized SEM images of a silicon scale suspended on the surface of a microtip stamp (a), printed photonic, plasmonic, and silicon scales on a PDMS substrate with center anchors (b), and printed silicon scales with edge anchors on a silicon substrate (c).

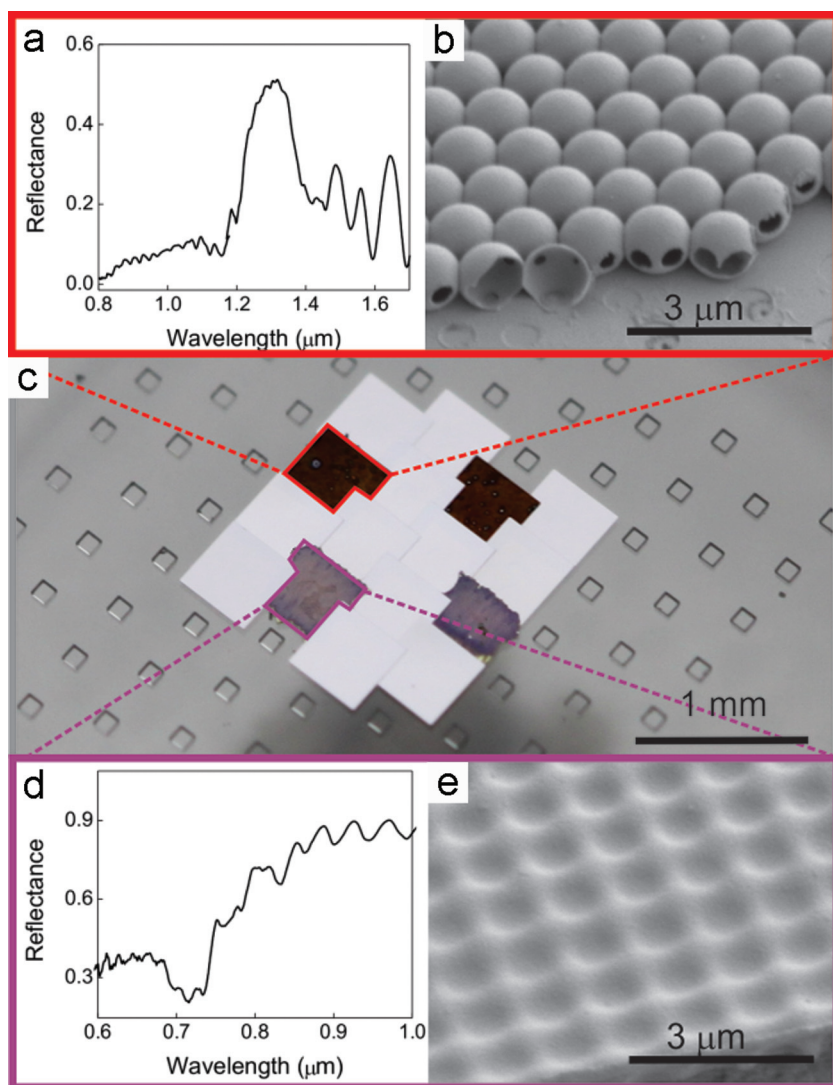


Figure 3. Specular reflectance spectra and SEM images obtained from printed photonic (a,b) and plasmonic (d,e) scales with center anchors on PDMS, shown in (c). Dashed lines indicate the scale from which the data was acquired.

realized through surface hydroxyl condensation reactions, as described in the Experimental Section. The lateral dimensions of the scales ($600\ \mu\text{m} \times 600\ \mu\text{m}$) exceeded the spacings between the posts ($500\ \mu\text{m}$), such that this assembly process yielded imbricate layouts with overlaps of $100\ \mu\text{m}$ for adjacent scales.

In a second design, scales with PDMS anchors located on one edge, prefabricated using procedures described in the Experimental Section, were printed onto flat silicon substrates. Here, the contact with the silicon occurs only at the anchors, which corresponds to an area more than 15 times smaller than that of the scales. This situation requires extremely low degree of adhesion to the stamp for efficient release in the printing process. The microtip design is critically important. **Figure 2a** presents a scanning electron microscopy (SEM) image of a representative stamp, ‘inked’ with a silicon scale, in the low-adhesion configuration. Here, the contact area between the microtip stamp and the silicon scale is extremely small. **Figure 2b** and **c** show SEM images

of imbricate architectures that use center and edge anchors, respectively. **Figure 3** presents an assembled structure consisting of a heterogeneous collection of silicon, photonic, and plasmonic scales, along with measured reflection spectra and magnified views of the structures. This construct shows remarkable degrees of bendability and stretchability, by virtue of the imbricate layout, the anchoring scheme and the elastomeric substrate. **Figure 4** shows images in various states of deformation, to illustrate this point. Large and varied strains, all with reversible behaviors are possible even with scales that are themselves rigid, brittle, and fragile (particularly the photonic crystal shells).

To test the mechanics in a more systematic way, we buckled and stretched a scaled surface laterally using translational stages to manipulate the clamped edges of the PDMS substrate. **Figure 5** provides optical images in a buckling mode (**Figure 5a**), a strain-free mode (**Figure 5b**), and a stretching mode (**Figure 5c**). The left frames show images of the scaled surface between two mechanical clamps. The right frames present magnified optical images and computed distributions of maximum principal strains in the scales for these three deformation modes. The dark areas between adjacent scales correspond to regions of spatial overlap (i.e., imbricate layout). Depending on the degree of deformation, these areas change in size, but they never completely disappear, for the cases shown here. Such behavior reveals that this architecture enables full, 100% effective area coverage, even under stretching, buckling, and bending. For the

deformation mode of **Figure 5a**, we laterally compressed the substrate to induce buckling that involved bending of the central region to a radius of $\sim 17\ \text{mm}$. At this level of bending, the scales maintain an imbricate layout without separation, thereby maintaining full coverage.

In these examples, the PDMS accommodates most of the dimensional change; each individual scale rotates, but retains its original flat geometry to good approximation. As a result, the surface can support rigid scales that, for the case of the plasmonic and photonic structures, retain their optical properties, similar to other approaches to strain-isolation design,^[22–23] but uniquely applicable to 100% surface area coverage, independent of deformation. To quantify related behavior, we measured the total length (L_0) between the two end clamps. When the scaled surface was stretched, the measured length between the clamps, L_1 , defines a characteristic strain value according to $(L_1 - L_0) / L_0$. This value is approximately 0.17 for **Figure 5c**. Optical microscopy indicates negligible effect of this strain on the geometry of the individual

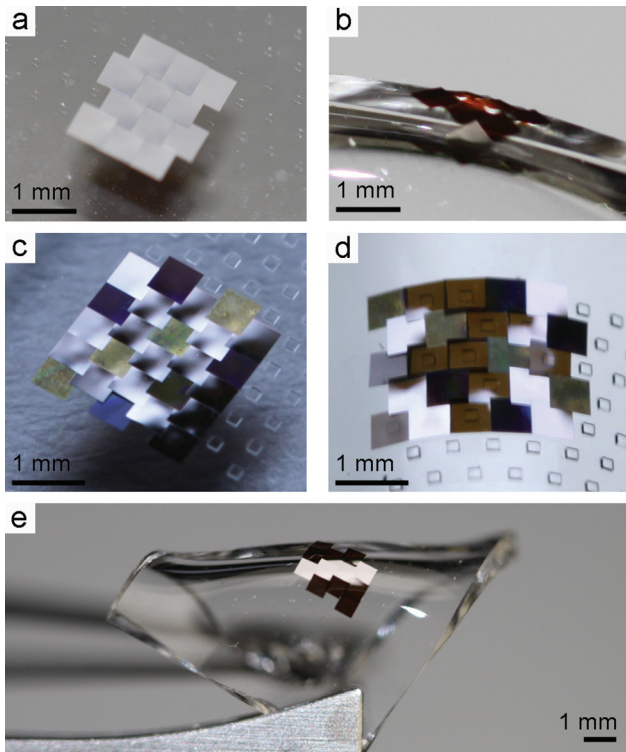


Figure 4. Optical images of homogeneous (silicon) (a,b) and heterogeneous (photonic, plasmonic, and silicon) (c,d) collections of scales with center anchors, on PDMS substrates in flat (a,c) and bending (b,d) modes. The appearance of the photonic and plasmonic scales changes with viewing angle. e) Optical image of homogeneous scales sample bent and twisted using a pair of tweezers.

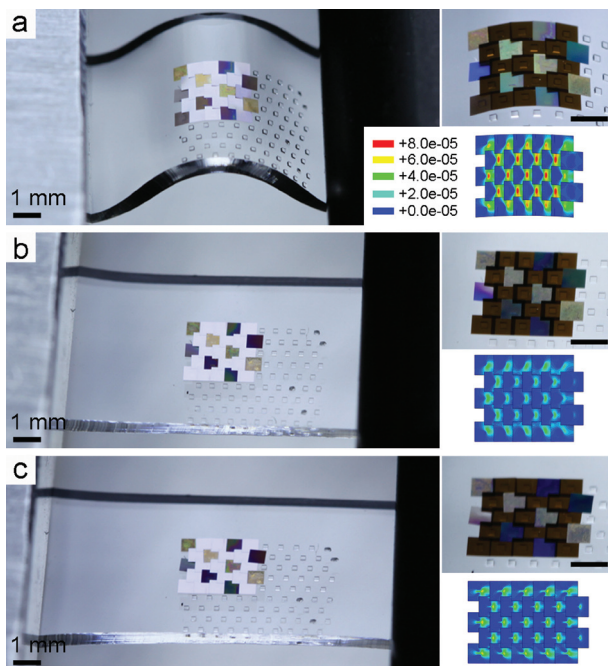


Figure 5. Optical images and finite element method (FEM) modeling results for a heterogeneous imbricate architecture of scales on a PDMS substrate with center anchors, bent to a 17 mm radius of curvature (a), in a flat, free-standing configuration (b), and stretched to 17% (c). The dark areas at the edges of the scales, visible in the right frames, correspond to overlapping regions (Scale bar: 1 mm).

scales. Such observations are consistent with FEM results in the right frames, which show extremely small strains in the scales, i.e., ~0.008%, 0.004%; and 0.006% for the buckling, strain-free; and stretching modes in experiments, respectively. Furthermore, the maximum of the principal strain in the scales is always reached at or near the posts.

3. Discussion

The mechanics of structures like those described above is critical to system design and understanding. A model, outlined in detail in the SI (Figure S3), gives the maximum strain ε_{\max} in the scales for the bending radius ρ and applied strain $\varepsilon_{\text{applied}}$ as

$$\varepsilon_{\max} = \frac{t_{\text{scale}}}{\rho} \frac{3(w_{\text{scale}} - w_{\text{post}}) [w_{\text{scale}} - (1 + \varepsilon_{\text{applied}}) s_{\text{post}}]}{6 [w_{\text{scale}} - (1 + \varepsilon_{\text{applied}}) s_{\text{post}}]^2 + 2 [w_{\text{post}} - (1 + \varepsilon_{\text{applied}}) s_{\text{post}}]^2} \quad (1)$$

which is linearly proportional to the scale thickness t_{scale} , inversely proportional to bending radius ρ , and also depends on the scale width w_{scale} , post width w_{post} , and spacing s_{post} . For the buckling mode that induces the bending radius $\rho = 17$ mm and $t_{\text{scale}} = 3$ μm , $w_{\text{scale}} = 600$ μm , $w_{\text{post}} = 140$ μm , and $s_{\text{post}} = 500$ μm as in experiments, the maximum strain in Equation 1 is 0.0076% for zero applied strain. This value agrees well with the FEM results (0.008%) in Figure 5a. Figure S3c (SI) shows the normalized maximum strain $\rho \varepsilon_{\max} / t_{\text{scale}}$ versus $w_{\text{scale}} / s_{\text{post}}$ for the applied strain ranging from 0 to 20%. All curves reach the same maximum value 3/4 such that an upper bound estimate of the maximum strain in the scales is

$$\varepsilon_{\max} = \frac{3t_{\text{scale}}}{4\rho} \quad (2)$$

An important design consideration relates to layouts that prevent the scales from collapsing onto the substrate, due to the action of generalized adhesion forces. The mechanics model in the SI (Figure S4) shows that, to prevent this collapse, the scale width w_{scale} must be less than a critical value given by

$$w_{\text{scale}} \leq w_{\text{post}} + 8 \left(\frac{2\overline{E}I_{\text{scale}}t_{\text{post}}^2}{9\gamma} \right)^{\frac{1}{4}} \quad (3)$$

where t_{post} is the post-thickness (Figure S4a, SI), $\overline{E}I_{\text{scale}}$ is the plane-strain bending stiffness of the scale, and γ is the adhesion energy of the interface between the scale and backing layer. Figure S4b,c (SI) shows that the scale width increases with the post and scale thicknesses, where $\overline{E}I_{\text{scale}} = \overline{E}_{\text{scale}}t_{\text{scale}}^3/12$ ($\overline{E}_{\text{scale}}$ —plane-strain modulus). For $t_{\text{post}} = 80$ μm , $\overline{E}_{\text{scale}} = 140$ GPa and other parameters in experiments, and $\gamma = 0.15$ J m⁻²,^[8] Equation 3 gives $w_{\text{scale}} \leq 2.01$ mm. The scale width in experiments $w_{\text{scale}} = 600$ μm , at which no collapse is observed, is indeed less than this critical value.

This width, however, has a lower limit necessary to ensure that the scales remain in imbricate configurations during large stretching and bending. The mechanics model in the SI (Figure S5) gives this minimal width as

$$w_{\text{scale}} \geq (2\rho + 2t_{\text{post}} + t_{\text{backinglayer}}) \tan \left[\frac{s_{\text{post}}}{2\rho} (1 + \varepsilon_{\text{applied}}) \right] \quad (4)$$

where $t_{\text{backinglayer}} = 0.8 \text{ mm}$ is the thickness of the backing layer. Figure S5c shows the normalized critical bending radius, ρ/s_{post} , below which the scales do not overlap, versus $w_{\text{scale}}/s_{\text{post}}$ for applied strains ranging from 0 to 20%. The critical bending radius is 2.45 mm for zero applied strain, and increases to 5.35 mm for $\varepsilon_{\text{applied}} = 10\%$. The bending radius in experiments $\rho = 17 \text{ mm}$, at which the scales remain in contact, is indeed larger than these critical values.

The normal and shear stress distribution at the scale-anchor interface is also given in the SI (Figure S6) when the scaled surface is under buckling or stretching modes.

4. Conclusion

This article reports a manufacturing route to imbricate microsystem architectures. The scales that we used here are designed for purposes of illustration. The same printing techniques have been used, in conventional, non-imbricate layouts, with microscale light-emitting diodes, photovoltaic cells, transistors, circuit blocks, and many other components. Applicability with such devices in imbricate layouts should also be possible, with interconnections potentially embedded in the anchor structures and underlying substrate. We believe also that more elaborate, 3D configurations could be interesting to examine. The mechanics models provide design guidelines for overlapping areas in imbricate layouts. Exploring some of these possibilities and exploiting them in functional devices with guidance from mechanics modeling represent topics of current work.

5. Experimental Section

Fabrication of Photonic and Plasmonic Surfaces: Two types of photonic surfaces were fabricated (Figure S7, SI). Photonic surface type A consisted of square arrays of cylindrical cavities etched on the top silicon layer of a silicon-on-insulator (SOI) wafer. The patterning process in this case exploited soft imprint lithography with molds of polydimethylsiloxane (PDMS) and 400 nm thick layers of a photocurable epoxy (2000.5 SU8 diluted by 8% wt. in cyclohexanol; MicroChem Corp.) formed by spin casting at 2000 rpm. Reactive ion etching (RIE) processes removed the residual layer of SU8 from the recessed regions of molded relief (3 min, 50 W, O_2 gas 10 sccm, 15 mTorr chamber pressure, rate 130 nm/min), and then the exposed, top silicon (1 min, 100 W, SF_6 gas 40 sccm, 50 mTorr chamber pressure, rate 1 $\mu\text{m}/\text{min}$) to a depth of $\sim 1 \mu\text{m}$. The remaining SU8 was removed by immersing the film in a piranha bath (3:1 vol. mixture of $\text{H}_2\text{SO}_4:\text{H}_2\text{O}_2$) for 1 h. Photonic surface type B consisted of single layers of hexagonally packed 600 nm diameter silicon shells. These scales were fabricated by spin-coating silica microspheres from an ethanolic

dispersion (20% wt., 4000rpm) onto an SOI wafer. Conformal coatings ($\sim 40 \text{ nm}$) of silicon were formed by chemical vapor deposition with disilane (Si_2H_6 , 98%, Gelest) in a single cycle (50 mbar, 3 h, 350 $^\circ\text{C}$, heating rate 8 $^\circ\text{C}/\text{min}$). The original silica microspheres were then removed by immersion in an HF bath (10% vol. aq.) for 1 h, followed by rinsing with ethanol and drying with N_2 .

Two types of plasmonic surfaces were fabricated (Figure S7). Plasmonic surface type A consisted of a 35 nm thick layer of Au (5 nm Cr adhesive layer) sputter-deposited onto Type A photonic scales. Plasmonic surface type B used Au deposited directly on top of imprinted layers of SU8.

Fabrication of Photonic, Plasmonic, and Silicon Scales: Photonic and plasmonic scales were derived from photonic or plasmonic surfaces preprocessed on SOI wafers (3 μm thick top silicon and 1.1 μm buried oxide, from Shin-Etsu Chemical Co., Ltd. and Soitec) according to procedures described above. Scales were defined in square layouts (600 $\mu\text{m} \times 600 \mu\text{m}$, square packing arrangement, 900 μm center-to-center separation) by patterning a layer of photoresist (AZ5214, 1.5 μm thick) and then etching the exposed layers (35 nm thick gold layer, silicon sphere monolayer, and/or silicon layer) consecutively. Etching with HF removed the buried oxide to generate an undercut trench below the periphery of the silicon squares. Next, the wafer was coated with photoresist (AZ5214, 1.5 μm thick) and flood-exposed with a dose of 150 mJ/cm². Immersion in developer (AZ 327 MIF) removed the photoresist everywhere except in the undercut regions; this remaining photoresist tethered the silicon squares to the underlying silicon wafer, at their edges, according to previously reported procedures.^[24] Finally, HF etching of the remaining oxide completed the process.

Fabrication of Scale Architectures with Center Anchors: Elastomeric substrates designed with center anchor relief structures were fabricated by casting and thermally curing (60 $^\circ\text{C}$ for 30 min) PDMS on the functionalized surface (trichlorosilane, United Chemical Technology) of a Si (100) wafer (Addison Engineering) with a pattern of SU-8 50 (80 μm thick, MicroChem Corp.) which provided square openings (140 $\mu\text{m} \times 140 \mu\text{m}$). Photonic, plasmonic, or silicon scales were retrieved from their donor substrates and printed onto the resulting posts. After printing the scales, the assembly was cured more fully (70 $^\circ\text{C}$ for 10 h) to yield strong interfacial bonding. Figure S2a (SI) provides a schematic illustration of the procedures.

Fabrication of Scale Architectures with Edge Anchors: A photolithographically defined pattern of SU-8 5 (15 μm thick, MicroChem Corp.) on a Si (100) wafer (Addison Engineering) provided rectangular openings (100 $\mu\text{m} \times 200 \mu\text{m}$). Prepolymer to PDMS was poured and scraped over the functionalized (trichlorosilane, United Chemical Technology) surface of this wafer,^[25] to define the dimensions of edge anchors made of PDMS. Silicon scales were printed on the partially cured surface of the PDMS (60 $^\circ\text{C}$ for 30 min). Fully curing the PDMS yielded strong bonding. These scales, with attached PDMS edge anchors, were then printed, together, onto a bare silicon substrate. Figure S2b provides a schematic illustration of the procedures.

Supporting Information

Supporting Information is available from the Wiley Online Library or from the author.

Acknowledgements

We thank Fredrick Larabee, Prof. Andrew V. Suarez, and the Illinois National History Survey Insect Collection for providing the *Morpho aega* butterfly specimen and for helping with the image capturing of the specimen. Financial support from NSF (Grant No. OISE-1043143) and from DARPA is acknowledged.

-
- [1] P. Vukusic, *Proc. R. Soc. B-Biol. Sci.* **1999**, 266, 1403.
 [2] R. Prum, T. Quinn, R. H. Torres, *J. Exp. Biol.* **2006**, 209, 748.
 [3] Y. Zheng, X. Gao, L. Jiang, *Soft Matter* **2007**, 3, 178.
 [4] J. Hazel, M. Stone, M. S. Grace, V. V. Tsukruk, *J. Biomech.* **1999**, 32, 477.
 [5] S. Foy, Oxford Scientific Films, in *The Grand Design: Form and Colour in Animals*, Prentice-Hall, **1983**, p.238.
 [6] R. Dudley, Oxford Scientific Films, in *The biomechanics of insect flight: form, function, evolution*, Princeton University Press, **2002**, p.118.
 [7] M. A. Meitl, Z.-T. Zhu, V. Kumar, K. J. Lee, X. Feng, Y.Y. Huang, I. Adesida, R. G. Nuzzo, J. A. Rogers, *Nat. Mater.* **2006**, 5, 33.
 [8] S. Kim, J. Wu, A. Carlson, S. H. Jin, A. Kovalsky, P. Glass, Z. Liu, N. Ahmed, S. L. Elgan, W. Chen, P. M. Ferreira, M. Sitti, Y. Huang, J. A. Rogers, *Proc. Natl. Acad. Sci. USA* **2010**, 107, 17095.
 [9] J. Yoon, A. J. Baca, S. I. Park, P. Elvikis, J. B. Geddes, L. Li, R. H. Kim, J. Xiao, S. Wang, T. H. Kim, M. J. Motala, B. Y. Ahn, E. B. Duoss, J. A. Lewis, R. G. Nuzzo, P. M. Ferreira, Y. Huang, A. Rockett, J. A. Rogers, *Nat. Mater.* **2008**, 7, 907.
 [10] M. J. Panzer, V. Wood, S. M. Geyer, M. G. Bawendi, V. Bulović, *J. Disp. Technol.* **2010**, 6, 90.
 [11] Z. Fan, H. Razavi, J. Do, A. Moriwaki, O. Ergen, Y.-L. Chueh, P. W. Leu, J. C. Ho, T. Takahashi, L. A. Reichertz, S. Neale, K. Yu, M. Wu, J. W. Ager, A. Javey, *Nat. Mater.* **2009**, 8, 648.
 [12] Sekitani T Someya, *Adv. Mater.* **2010**, 22, 2228.
 [13] H. Kim, E. Brueckner, J. Song, Y. Li, S. Kim, C. Lu, J. Sulking, K. Choquette, Y. Huang, R.G. Nuzzo, J.A. Rogers, *Proc. Natl. Acad. Sci. USA* **2011**, 108, 10072.
 [14] T. Sekitani, H. Nakajima, H. Maeda, T. Fukushima, T. Aida, K. Hata, T. Someya, *Nat. Mater.* **2009**, 8, 494.
 [15] J. Lee, J. Wu, M. Shi, J. Yoon, S.-I. Park, M. Li, Z. Liu, Y. Huang, J.A. Rogers, *Adv. Mater.* **2011**, 23, 986.
 [16] C. E. Packard, A. Murarka, E. W. Lam, M. A. Schmidt, V. Bulović, *Adv. Mater.* **2010**, 22, 1840.
 [17] Y. Qi, J. Kim, T. D. Nguyen, B. Lisko, P. K. Purohit, M. C. McAlpine, *Nano Lett.* **2011**, 11, 1331.
 [18] K. Takei, T. Takahashi, J. C. Ho, H. Ko, A. G. Gillies, P. W. Leu, R. S. Fearing, A. Javey, *Nat. Mater.* **2010**, 9, 821.
 [19] T. Takahashi, K. Takei, E. Adabi, Z. Fan, A. M. Niknejad, A. Javey, *ACS Nano* **2010**, 4, 5855.
 [20] NationalGeographicwebsite, <http://www.nationalgeographicstock.com/>, Picture ID:1157722. Accessed: July, 2011.
 [21] X. Feng, M. A. Meitl, A. M. Bowen, Y. Huang, R. G. Nuzzo, J. A. Rogers, *Langmuir* **2007**23, 12555.
 [22] D.-H. Kim, Y.-S. Kim, J. Wu, Z. J. Liu, J. Z. Song, H.-S. Kim, Y. Huang, K.-C. Hwang, J. A. Rogers, *Adv. Mater.* **2009**, 21, 1.
 [23] H. Cheng, J. Wu, M. Li, D.-H. Kim, Y.-S. Kim, Y. Huang, Z. Kang, K. C. Hwang, J. A. Rogers, *Appl. Phys. Lett.* **2011**, 98, 061902.
 [24] Y. Yang, Y. Hwang, H. A. Cho, J.-H. Song, S.-J. Park, J. A. Rogers, H. C. Ko, *Small* **2011**, 7, 484.
 [25] M. J. Kim, J. Yoon, S.-I. Park, J. A. Rogers, *Appl. Phys. Lett.* **2009**, 95, 214101.

Received: September 3, 2011
 Published online: December 19, 2011